



# Polymer nano-composite films with inorganic upconversion phosphor and electro-optic additives made by concurrent triple-beam matrix assisted and direct pulsed laser deposition



Abdalla M. Darwish<sup>a,\*</sup>, Shaelynn Moore<sup>a</sup>, Aziz Mohammad<sup>a</sup>, Deonte' Alexander<sup>a</sup>, Tyler Bastian<sup>a</sup>, Wydglif Dorlus<sup>a</sup>, Sergey Sarkisov<sup>b</sup>, Darayas Patel<sup>c</sup>, Paolo Mele<sup>d</sup>, Brent Koplitz<sup>e</sup>, David Hui<sup>f</sup>

<sup>a</sup> Physics Department, Dillard University, New Orleans, LA 70122, USA

<sup>b</sup> SSS Optical Technologies, 515 Sparkman Drive, Huntsville, AL 35816, USA

<sup>c</sup> Oakwood University, Department of Mathematics & Computer Science, 7000 Adventist Blvd, Huntsville, AL 35896, USA

<sup>d</sup> Muroran Institute of Technology College of Design and Manufacturing Technology Research Center for Environmentally Friendly Materials Engineering, 27-1 Mizumoto-cho, Muroran, Hokkaido, 050-8585, Japan

<sup>e</sup> Chemistry Department, Tulane University, New Orleans, LA 70122, USA

<sup>f</sup> Mechanical Engineering Department, University of New Orleans, New Orleans, LA 70148, USA

## ARTICLE INFO

### Article history:

Received 5 September 2016

Accepted 19 October 2016

Available online 20 October 2016

### Keywords:

Nano-composite polymer films

Pulsed laser deposition

Matrix assisted pulsed laser evaporation

Rare earth upconversion phosphors

Multiple beam multiple target pulsed laser deposition

## ABSTRACT

The work was to investigate polymer nano-composite films with two inorganic additives: upconversion fluorescent phosphor  $\text{NaYF}_4:\text{Yb}^{3+}, \text{Er}^{3+}$  and aluminum doped ZnO (AZO). The films were deposited using a new method of concurrent evaporation of the frozen solution of polymer poly(methyl methacrylate) (PMMA) using the matrix assisted pulsed laser evaporation (MAPLE) and the ablation of the phosphor and AZO targets using the pulsed laser deposition (PLD). Three laser beams, an infrared 1064-nm beam for the MAPLE and two 532-nm beams for the PLD targets, were concurrently used in the process. A new target holder with remote control of the target tilt was designed to provide overlapping of the plumes from the three targets and uniform mixing of the additives in the polymer film. The fabricated nano-composite films were characterized using X-ray diffraction, scanning electron microscopy (SEM), and the measurement of the quantum efficiency (QE) of the upconversion fluorescence. The films retained the crystalline structure of the inorganic additives. The size of the nano-particles varied in the range 10–200 nm. Upconversion QE of the films was an order of magnitude less than that of the bulk phosphor, which can be explained by lesser number of the rare-earth ions in the nano-particles in the polymer film than in the micro-grains of the bulk phosphor. The AZO additive increased QE by 1.6 times to  $(0.072 \pm 0.022) \%$  more likely due to the plasmonic enhancement of the local optical infra-red pump (980 nm) field. The proposed triple-beam triple-target MAPLE/PLD method can be potentially used for making a wide variety of nano-composite films.

© 2016 Elsevier Ltd. All rights reserved.

## 1. Introduction

There has been an explosive interest in the technique of laser assisted deposition of polymer nano-composite films exploiting the matrix assisted pulsed laser evaporation (MAPLE) with regard to the polymer host as can be judged from the numerous recent publications [1–40]. In MAPLE, a frozen solution of a polymer in a

relatively volatile solvent is used as a laser target. The solvent and concentration are selected so that first, the polymer of interest can dissolve to form a dilute, particulate free solution, second, the majority of the laser energy is initially absorbed by the solvent molecules and not by the solute molecules, and third, there is no photochemical reaction between the solvent and the solute. The light-material interaction in MAPLE can be described as a photo-thermal process. The photon energy absorbed by the solvent is converted to thermal energy that causes the polymer to be heated but the solvent to vaporize. As the surface solvent molecules are evaporated into the gas phase, polymer molecules are exposed at

\* Corresponding author.

E-mail address: [adarwish@bellsouth.net](mailto:adarwish@bellsouth.net) (A.M. Darwish).

the gas-target matrix interface. The polymer molecules attain sufficient kinetic energy through collective collisions with the evaporating solvent molecules, to be transferred into the gas phase. By careful optimization of the MAPLE deposition conditions (laser wavelength, repetition rate, solvent type, concentration, temperature, and background gas and gas pressure), this process can occur without any significant polymer decomposition. The MAPLE process proceeds layer-by-layer, depleting the target of solvent and polymer in the same concentration as the starting matrix. When a substrate is positioned directly in the path of the plume, a coating starts to form from the evaporated polymer molecules, while the volatile solvent molecules are evacuated by the pump from the deposition chamber. In case of fabrication of polymer nanocomposites, MAPLE targets are usually prepared as nano-colloids of the additives of interest in the initial polymer solutions.

Mixing the components of different nature, organic polymers and inorganic dopants, in the same target at a certain proportion and exposing them to the same laser beam not necessarily brings good quality nano-composite films. The laser pulse energy and wavelength cannot be optimized for each component individually. Also, the mixing proportion in the composite film is dictated by the initial proportion of the target and thus cannot be changed in the process. These limitations were removed in the recently proposed method of multi-beam and multi-target deposition (in its double-beam/dual-target variation) using a MAPLE polymer target and one inorganic target, each being concurrently exposed to laser beams of different wavelengths [41–50]. Using the method, nano-composite films of polymer poly(methyl methacrylate) known as PMMA doped with a rare earth (RE) inorganic upconversion phosphor compounds were prepared. Also, a nano-composite film of thermoelectric film of inorganic aluminum-doped ZnO known as AZO was impregnated with PMMA nano-fillers with the purpose of improving electrical conductivity and thermoelectric performance [46,50]. The polymer target was a frozen (to a temperature of liquid nitrogen) PMMA solution in chlorobenzene exposed to a 1064-nm laser beam from a Q-switched Nd:YAG pulsed laser. The inorganic targets were the pellets made of the compressed micro-powders of highly efficient RE-doped  $\text{NaYF}_4$  or the sintered powder of AZO concurrently ablated with the conventional pulsed laser deposition (PLD) process using the 532-nm frequency doubled beam from the same laser. The major result was that both, the polymer and the inorganic components could be transferred on a substrate during the combined MAPLE/PLD process in the form of a uniformly mixed nano-composite film preserving the chemical/crystalline structure of the components and with the desired new functional properties (highly efficient upconversion emission or the improved thermoelectric energy harvesting). The early work was limited to two laser beams and two targets (polymer MAPLE and inorganic PLD). Also, the target tilt (in order to provide overlapping of the plumes from both targets on the substrate) was adjusted manually inside the open vacuum chamber before the deposition process. Any correction of the plume directions in order to optimize the overlapping required time consuming operations of opening the chamber followed by degassing and reaching high vacuum. This paper presents the results of the further improvements of the proposed method. The number of the laser beams and the targets is increased to three: one polymer MAPLE and two inorganic PLD targets. The MAPLE target is the frozen solution of PMMA. The inorganic targets are made of an upconversion phosphor and aluminum doped oxide ZnO known as AZO. The targets are tilted remotely without opening the chamber in such a way that the plume overlapping can be optimized during the deposition process. The focus is on preserving the chemical and crystalline structure of the components in the resulting polymer nano-composite films with two inorganic additives and gaining the functionalities attributed to the additives and

their interaction with the polymer host and with each other.

## 2. Methods and materials

### 2.1. Triple-beam triple-target MAPLE/PLD system with remotely controlled target tilting

The design of the proposed triple-beam triple-target deposition system (for the sake of simplicity presented for two beams and two targets) is shown in Fig. 1. Remotely controlled vacuum compatible linear actuators tilt the targets in order to achieve an optimal angle  $\theta$  between the plumes (which are perpendicular to the target surfaces) at which the plumes overlap on the surface of the substrate. This secures the uniform mixing of the materials from the targets in the composite film during the deposition process. The images of the tilt control sub-system for three targets are presented in Figs. 2 and 3. One important advantage of this sub-system as compared to the previous double-beam PLD system [41–50] is that the target holders are tilted around the axes in the horizontal plane instead of vertical plane, which prevents from dropping or spilling the target material.

One of the target holders of the above-mentioned triple-target sub-system is designed to accommodate a MAPLE target cooled with flowing liquid nitrogen (LN) as presented in Figs. 4 and 5. A copper container (cup) for a polymer solution is mounted on a copper container for LN (the cooler) that will be cooling the polymer solution (the target) and keeping it frozen. The MAPLE target assembly is connected to the LN feeding and collecting lines (copper tubing) drawn through a flange to be attached to the vacuum chamber. The feeding line is connected to the LN feeding vessel external to the vacuum chamber. The collecting LN line is

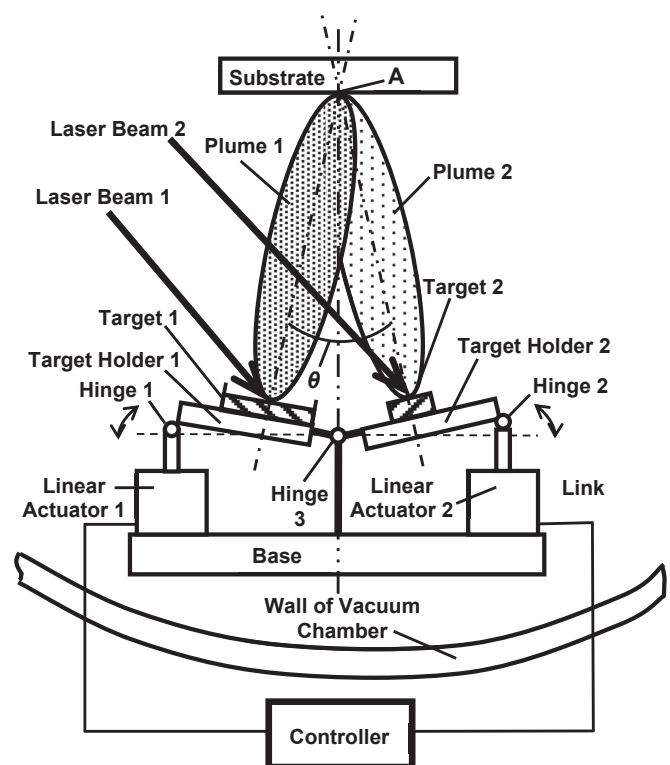
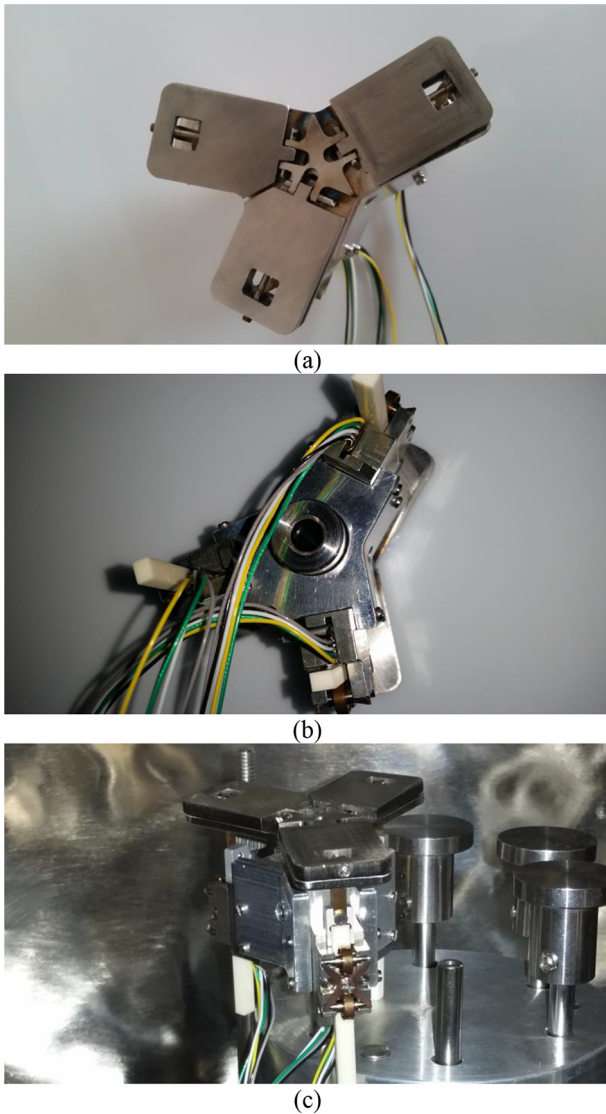


Fig. 1. Schematic of the target tilting sub-system of the new multi-beam multi-target PLD/MAPLE system with remote control of the directions of the plumes. Shown are two targets out of three.  $\theta$  is the optimal angle between the plumes when they overlap in point A on the surface of the substrate.



**Fig. 2.** Photographs of the three-target tilt control sub-system: (a) top view; (b) bottom view; (c) side view of the sub-system installed in the vacuum chamber.

connected to another external vessel where the LN flows in after passing through the cooler. The MAPLE target assembly is mounted on the top of one of the tilting target holders (Figs. 2–3) installed inside the vacuum chamber. Again, horizontal orientation of the MAPLE target in the new design made possible to conveniently install the empty copper cup in the chamber and fill it later with the liquid polymer solution without the risk of spilling it out before freezing.

## 2.2. Upconversion phosphor target

The first inorganic PLD target was made by compressing a powder of efficient upconversion phosphor  $\text{NaYF}_4:\text{Yb}^{3+}, \text{Er}^{3+}$  with a 25-ton hydraulic press. Detailed description of the synthesis of the phosphor and its properties was provided in the previous publications of the authors [41–49]. Frequency upconversion, or just upconversion, phosphor is a material that absorbs low-frequency (low photon energy) optical radiation, such as infra-red (IR) and re-emits high frequency (high photon energy) radiation, such as visible. The compounds containing the ions of the rare

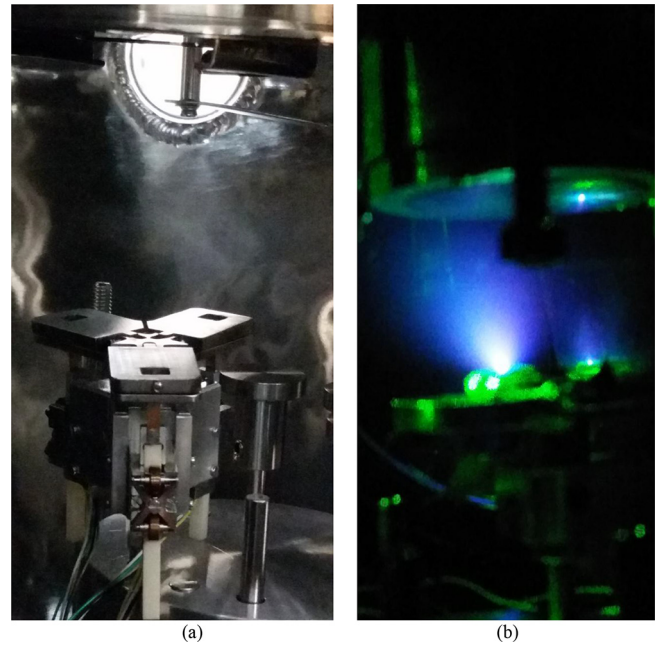


**Fig. 3.** Photographs of the three-target sub-system: side close-up view of the sub-system installed in the vacuum chamber (a); side view of the plumes emanating from two targets (out of three) during the PLD process.

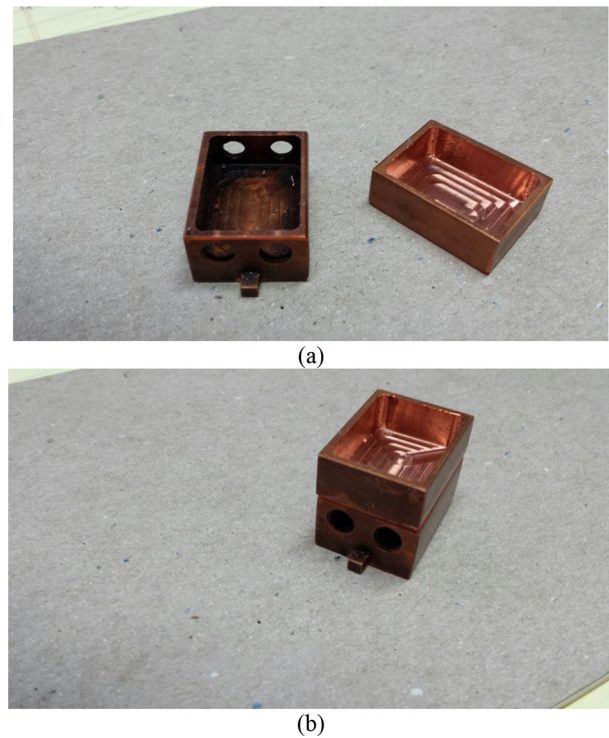


**Fig. 4.** Photographs of the MAPLE cooling sub-system: (a) liquid nitrogen chamber (left) and the polymer solution MAPLE cup (right); (b) the polymer solution MAPLE cup sits on the top of the cooling liquid nitrogen chamber (bottom).

earth (RE) elements, such as erbium, are particularly interesting as upconversion phosphors, since they have demonstrated good quantum efficiency (up to 5%). The upconversion efficiency greatly depends on the host for the RE ions. Popular modern highly efficient upconversion phosphors use hexagonal beta-phase crystalline fluoride  $\text{NaYF}_4$  ( $\beta\text{-NaYF}_4$ ) as the host material due to the

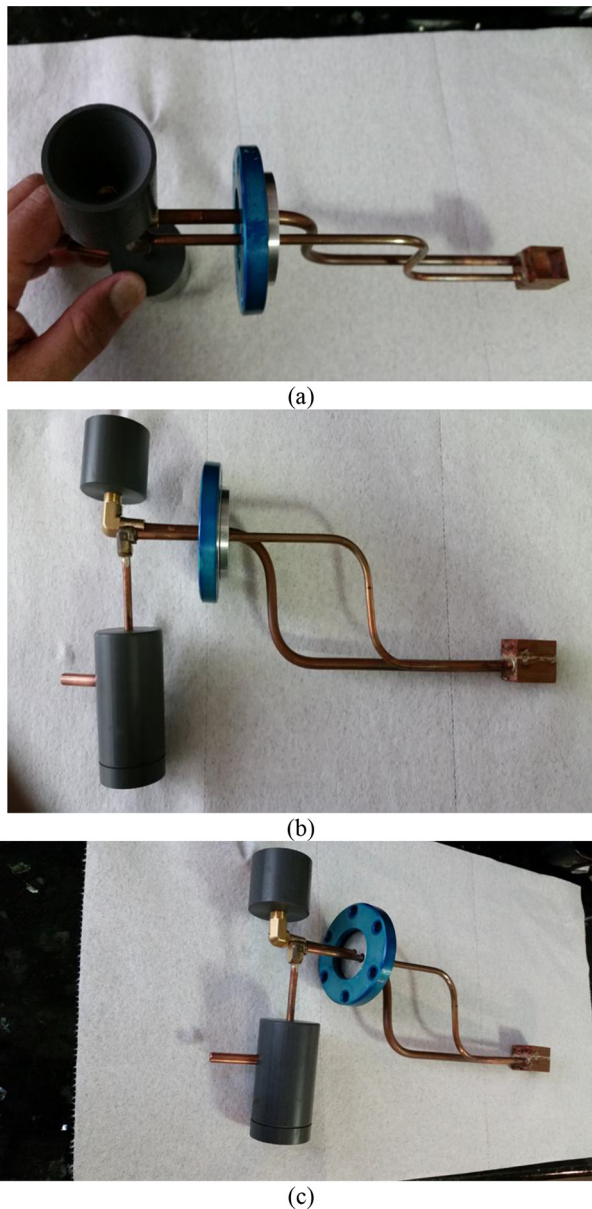


**Fig. 5.** Photographs of the MAPLE cooling sub-system: (a) top/side view of the liquid nitrogen cooled MAPLE target with accessories; (b) side view; (c) top-side view.

low phonon energy of the crystal lattice that minimizes the non-radiative multi-phonon relaxation process of the excited RE dopants. The powder of phosphor  $\text{NaYF}_4:\text{Yb}^{3+}, \text{Er}^{3+}$  with the doping rates of  $\text{Yb}^{3+}$  and  $\text{Er}^{3+}$  10% and 2% respectively (ten ytterbium ions and two erbium ions per 100 ions of sodium), was synthesized using the wet method [41] and baked for one hour at  $400^\circ\text{C}$  in open air to convert host  $\text{NaYF}_4$  in its hexagonal crystalline  $\beta$ -phase and maximize the upconversion efficiency. The phosphor powder produced intense visible upconversion emission with two green spectral peaks at 515 and 535 nm and one red spectral peak at 653 nm being pumped with infra-red (980 nm) radiation from a laser diode [41,43]. Fig. 6 presents the X-ray diffraction spectrum of the phosphor powder taken with Bruker D2 Phaser X-ray diffractometer. All the observed diffraction peaks can be attributed to  $\beta$ - $\text{NaYF}_4$  thus indicating that this is the dominating crystalline phase of the powder.

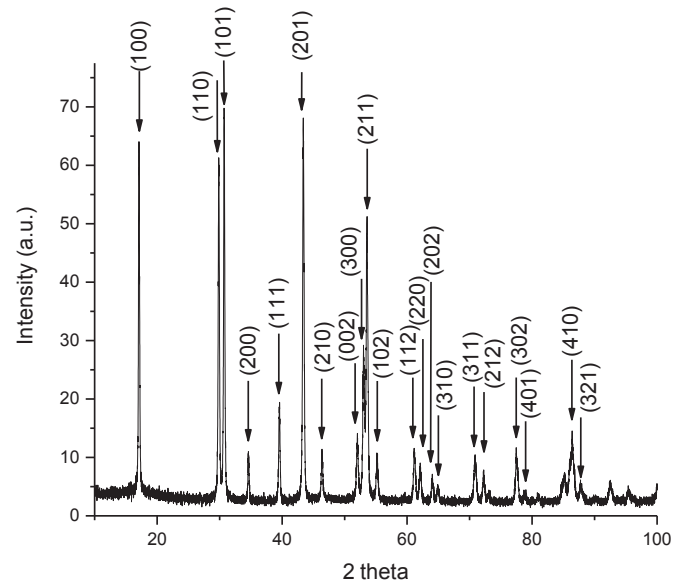


**Fig. 6.** XRD spectra of the upconversion powder baked for one hour at  $400^\circ\text{C}$  with the diffraction peaks attributed to the hexagonal  $\beta$ -phase of  $\text{NaYF}_4$ .

### 2.3. AZO target

AZO compound has recently attracted attention as an optically transparent electric conductor with the surface plasmon resonance (SPR) enhancement of local optical field similar to the noble metals, but without significant optical losses attributed to them [51–54]. It can thus be expected that adding AZO nano-particles to the upconversion phosphor in a polymer nano-composite film will bring the local enhancement of the pumping IR optical field in the vicinity of the phosphor nano-particles and consequently the increase of the intensity of the upconversion emission. PLD target was a pellet of  $\text{Zn}_{0.98}\text{Al}_{0.02}\text{O}$  where the Aluminum fraction was 2% of the total by weight as compared with zinc, not counting the oxygen. The AZO pellet had 20 mm in diameter and 3 mm in thickness. The pellet was prepared by Spark Plasma Sintering (SPS), also referred to as Pulsed Electric Current Sintering (PECS). In SPS pulsed DC current passed through a graphite die, as well as the AZO powder compact. Joule heating played a dominant role in the densification of the powder compact, which resulted in achieving near theoretical density at a lower sintering temperature compared to conventional sintering techniques. The heat generation is internal, in contrast to the conventional hot pressing, where the heat is provided by external heating elements. This facilitated a very high heating or cooling rate (up to 1000 K/min), hence the sintering process was very fast (within a few minutes). The general speed of the process ensured it densified the powder without coarsening, which accompanied standard densification routes. While the term “spark plasma sintering” is commonly used, a literal interpretation of the term may be misleading since neither a spark nor a plasma is present in the process. Fig. 7 presents the X-ray diffraction spectrum of the AZO target taken with Bruker D2 Phaser X-ray diffractometer. All the observed diffraction peaks can be attributed to  $\text{ZnO}$ .

### 2.4. Deposition procedure

A sample of the solution of poly(methyl methacrylate) known as PMMA in chlorobenzene at a proportion of 1.0 g solids per 10 mL liquids was poured in a copper cup of the MAPLE target assembly

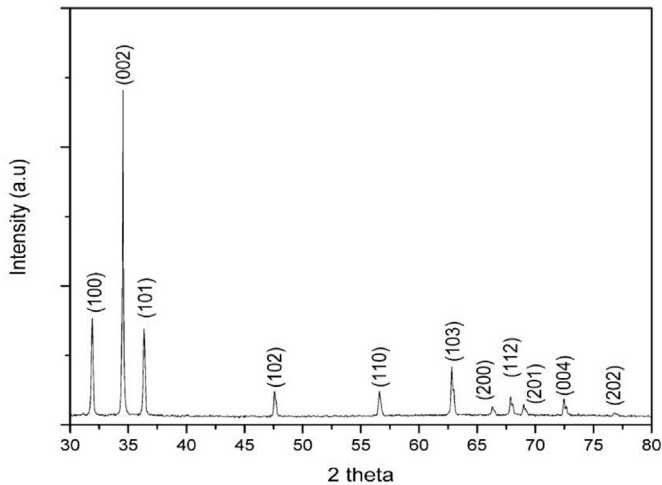


Fig. 7. XRD spectra of the prepared AZO PLD target with the diffraction peaks attributed to ZnO.

(Fig. 4) and frozen in liquid nitrogen. The second (PLD) target was the pellet of the upconversion phosphor. The third (PLD) target was the AZO pellet. Two pulsed laser sources were used. The first source was a Spectra Physics Quanta Ray Nd:YAG Q-switched Pro-250-50 laser with a pulse repetition rate of 50 Hz, 750-mJ energy per pulse at the 1064-nm fundamental wavelength, and 400-mJ energy per pulse at the 532-nm second harmonic. The second laser source (synchronized with the first source) was a Spectra Physics Quanta Ray Nd:YAG Q-switched Lab-170-10 laser with a pulse repetition rate of 10 Hz, 850-mJ energy per pulse at the 1064-nm fundamental wavelength and 450-mJ energy per pulse at the 532-nm second harmonic. The first (MAPLE) target was evaporated with the 1064-nm laser beam from the first source and exposed to the fluence ranging from 0.84 to 2.4 J/cm<sup>2</sup> per pulse. The second (PLD) target was concurrently ablated with the 532-nm frequency doubled Nd:YAG beam from the same source. The fluence was tuned up

between 0.8 and 1.0 J/cm<sup>2</sup> to keep the proportion of the upconversion material in the polymer film at approximately 5% by weight. The third (PLD) target was concurrently ablated with the 532-nm frequency doubled Nd:YAG beam from the second source. The fluence was tuned up between 1.0 and 2.2 J/cm<sup>2</sup> to keep the proportion of the upconversion material in the polymer film at approximately 5% by weight. The polymer films were deposited on preoxidized Si (100) substrates (until the second target) with a SiO<sub>2</sub> layer thickness of 2.0 μm. The deposition time was ~3.0 min (until the second target) started showing the signs of erosion. The thickness of the deposited films was between 180 and 200 nm as measured with an Atomic Force Microscope.

### 3. Results and discussion

#### 3.1. Crystalline structure of the inorganic additives in the polymer nano-composite film

In order to conduct X-ray diffraction spectroscopy, the films were removed from the substrates and placed in the Bruker D2 Phaser X-ray diffractometer. A reference sample of the PMMA nano-composite film containing only one upconversion phosphor additive was also made. The X-ray diffraction spectrum of this sample is presented in Fig. 8. The spectrum has all the signatures of the hexagonal β-phase NaYF<sub>4</sub> that was initially present in the second (PLD) target made of the upconversion phosphor. Since polymer PMMA is an amorphous material, it did not produce any sharp, high intensity X-ray diffraction peaks [55]. Accordingly, its contribution to the X-ray diffraction pattern of the polymer nano-composite could be neglected. Fig. 9 shows the X-ray diffraction spectrum of the polymer-nanocomposite film including nanoparticles of both inorganic additives: the upconversion phosphor and AZO. The observed spectral peaks include those that can be attributed to both β-phase NaYF<sub>4</sub> and AZO. It thus can be concluded that the two inorganic additives have been transferred to the polymer film without modification of their crystalline structure during the PLD process.

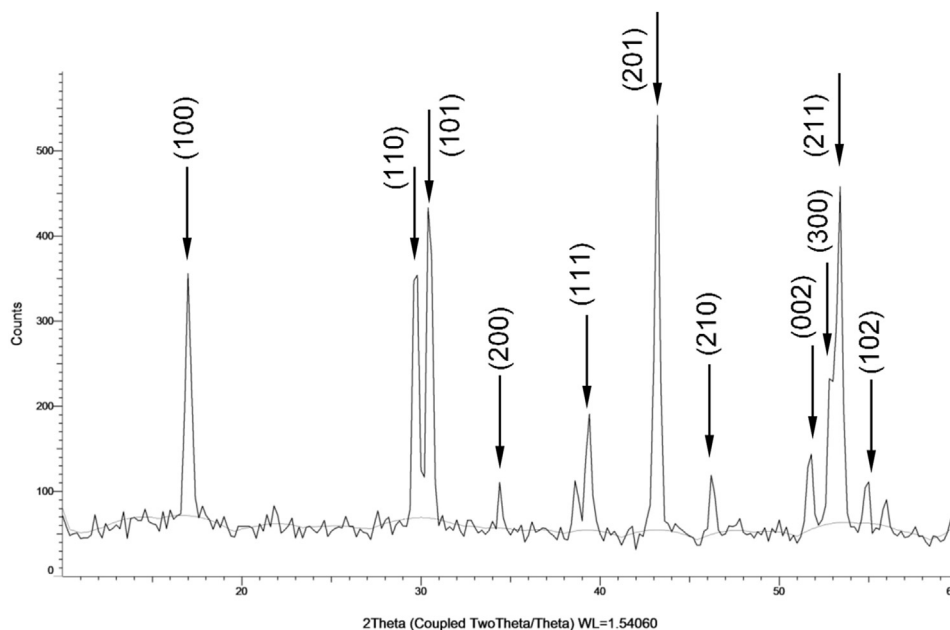


Fig. 8. XRD spectrum of the two-component composite film made of PMMA and the nanoparticles of NaYF<sub>4</sub>: Yb<sup>3+</sup>, Er<sup>3+</sup> with the diffraction peaks attributed to the hexagonal β-phase of NaYF<sub>4</sub>.

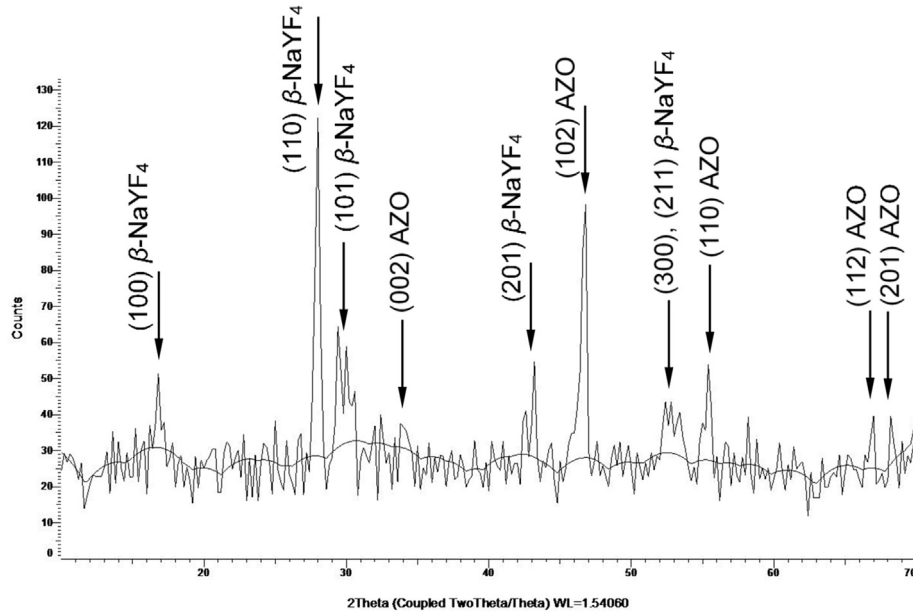


Fig. 9. XRD spectrum of the three-component composite film made of PMMA and the nanoparticles of NaYF<sub>4</sub>: Yb<sup>3+</sup>, Er<sup>3+</sup> and AZO.



Fig. 10. Scanning electron microscopy (SEM) image of the three-component composite film made of PMMA and the nanoparticles of NaYF<sub>4</sub>: Yb<sup>3+</sup>, Er<sup>3+</sup> and AZO with magnification  $\times 40000$ . White arrows point to exemplary nanoparticles of various sizes embedded in the polymer matrix.

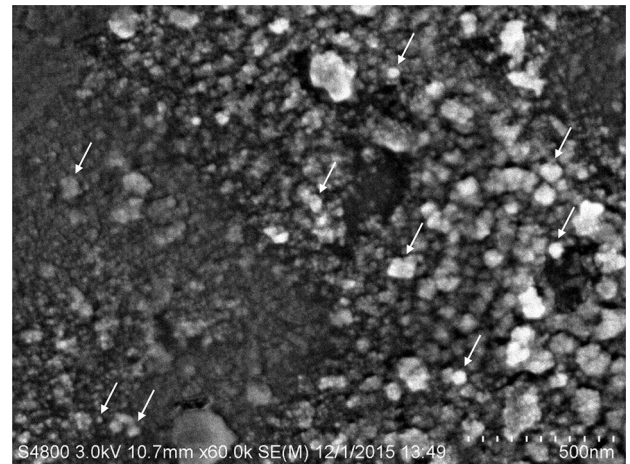


Fig. 11. Scanning electron microscopy (SEM) image of the three-component composite film made of PMMA and the nanoparticles of NaYF<sub>4</sub>: Yb<sup>3+</sup>, Er<sup>3+</sup> and AZO with magnification  $\times 60000$ . White arrows point to exemplary nanoparticles of various sizes (from  $\sim 10$  to 200 nm) embedded in the polymer matrix.

### 3.2. Nano-composite structure

Figs. 10 and 11 present the photographs of the high-resolution scanning electron images of the produced nano-composite film with a magnification of  $\times 40K$  and  $\times 60K$  respectively. For the sake of convenience, the images of some exemplary nanoparticles are marked with arrows. The size of the nanoparticles varied widely in the range between 10 and 200 nm. The nearly uniform distribution of the nanoparticles in the polymer film was occasionally disrupted by nano-particulate clusters of 500–1000 nm in size.

### 3.3. Fluorescence

The deposited nano-composite films demonstrated visible upconversion fluorescence being pumped with a 980-nm IR radiation. The spectrum of the upconversion emission resembled the

spectrum of the bulk upconversion phosphor with two green spectral peaks at 515 and 535 nm and one red spectral peak at 653 nm in the agreement with the results reported earlier [41,43]. The upconversion fluorescence of the films was quantitatively characterized by quantum efficiency (QE)  $\eta$  defined as the ratio of the number of the photons of the short-wavelength upconversion radiation generated per unit of time  $n_{up}$  to the number of the photons of the infra-red pump radiation  $n_{pump}$  [56]

$$\eta = \frac{n_{up}}{n_{pump}} 100\% \quad (1)$$

Fig. 12 presents the schematic of the experimental setup used to estimate QE. The film specimen was illuminated with a collimated beam from a fiber terminated 980-nm laser diode. The beam was normal to the specimen. The total power of the pump beam  $P_{pump\ tot}$

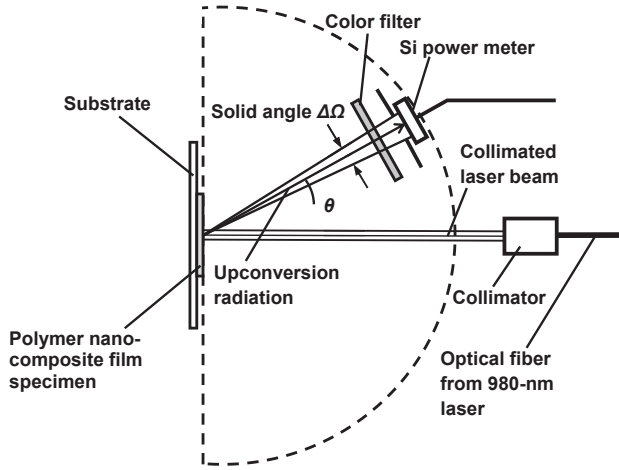


Fig. 12. Schematic of the optical setup for measuring the quantum yield (QE) of the upconversion emission from the prepared polymer nano-composite films containing phosphor  $\text{NaYF}_4: \text{Yb}^{3+}, \text{Er}^{3+}$ .

was fixed at 150 mW. Upon striking the specimen the beam initiated an upconversion emission. A Si power meter with the sensor aperture diameter  $d = 8$  mm was placed at distance  $L = 68$  mm from the specimen at angle  $\theta \sim 45^\circ$  with respect to the normal. Both the pump and the upconversion radiation were scattered out by the specimen within the hemisphere above its surface. Assuming that the specimen was a Lambertian emitter, one could determine what fraction  $F$  of the total scattered radiation was propagating towards the sensor of the power meter:

$$F = \frac{P_{\text{scatt pump}}}{P_{\text{scatt pump tot}}} = \frac{P_{\text{up}}}{P_{\text{up tot}}} = \frac{\Delta\Omega \cos\theta}{\pi} = \frac{\cos\theta}{4} \left(\frac{d}{L}\right)^2 \sim \frac{1}{4\sqrt{2}} \left(\frac{d}{L}\right)^2 = 2.45 \times 10^{-3} \quad (2)$$

where  $P_{\text{scatt pump tot}}$  is the power of the total pump radiation scattered out in the hemisphere;  $P_{\text{scatt pump}}$  is the power of the scattered pump IR radiation propagating towards the sensor aperture;  $P_{\text{up tot}}$  is the total power of the upconversion radiation scattered in the hemisphere;  $P_{\text{up}}$  is the power of the upconversion radiation propagating towards the sensor aperture;  $\Delta\Omega = \frac{1}{4}(d/L)^2$  is the solid angle formed by the sensor aperture within which the radiation (IR and upconversion) scattered from the specimen propagated towards the sensor. Since the power of the scattered pump radiation  $P_{\text{scatt pump}}$  was many orders of magnitude greater than  $P_{\text{up}}$ , the power meter measured mainly  $P_{\text{scatt pump}}$  and the contribution from  $P_{\text{up}}$  could be neglected. In order to measure  $P_{\text{up}}$  a green color filter (bandpass,  $540 \pm 20$  nm) was placed in front of the sensing element of the power meter to block the pump IR radiation. The transmittance of the color filter for the pump radiation was  $T_{\text{pump}} = 3.8 \times 10^{-4}$ ; transmittance for the upconversion radiation (at 535 nm) was  $T_{\text{up}} = 0.106$ . Power of the scattered pump radiation  $P_{\text{scatt pump filter}}$  passing through the filter in the sensor could thus be estimated as

$$P_{\text{scatt pump filter}} = P_{\text{scatt pump}} T_{\text{pump}} \quad (3)$$

Power of the combined pump and upconversion radiation measured by the power meter with the color filter in front of its sensor  $P_{\text{PM filter}}$  was thus

$$P_{\text{PM filter}} = P_{\text{up}} T_{\text{up}} + P_{\text{scatt pump filter}} \quad (4)$$

Using Eq. (2) through (4) the total power of the upconversion radiation  $P_{\text{up tot}}$  was estimated as

$$P_{\text{up tot}} = \frac{P_{\text{PM filter}} - P_{\text{scatt pump}} T_{\text{pump}}}{F T_{\text{up}}} \quad (5)$$

Using Eq. (2) the pump power consumed for the generation of upconversion radiation was estimated as

$$P_{\text{pump}} = P_{\text{pump tot}} - \frac{P_{\text{scatt pump}}}{F} \quad (6)$$

The number of photons per unit of time  $n$  was related to the power of radiation  $P$  as

$$n = \frac{P\lambda}{hc} \quad (7)$$

where  $\lambda$  was the wavelength;  $h$  was the Planck's constant; and  $c$  was the speed of light in vacuum ( $3 \times 10^8$  m/s). Accordingly, the number of pump and upconversion photons per unit of time related to the respective powers could be expressed as

$$n_{\text{up}} = \frac{P_{\text{up tot}} \lambda_{\text{up}}}{hc} \quad (8)$$

and

$$n_{\text{pump}} = \frac{P_{\text{pump}} \lambda_{\text{pump}}}{hc} \quad (9)$$

Based on Eqs. (1), (8) and (9) QE was computed as

$$\eta = \frac{P_{\text{up tot}} \lambda_{\text{up}}}{P_{\text{pump}} \lambda_{\text{pump}}} 100\% \quad (10)$$

The values of the estimated quantum efficiencies of green (at 515 and 535-nm spectral peaks combined) upconversion of the deposited polymer nano-composite films (with the phosphor only and with the phosphor and the AZO additive) together with the phosphor PLD target (as a reference) are presented in Table 1. The measured QE of the bulk phosphor powder compressed in the PLD target compared well against the highest 3% quantum yield reported for similar upconversion phosphor  $\text{NaYF}_4: \text{Yb}^{3+}, \text{Er}^{3+}$  in the literature [56]. The QE of the polymer nano-composite film containing only the nano-particles of the upconversion phosphor was  $\sim 12$  times less than that of the reference. On the other side, the nano-composite film deposited under similar conditions, but also containing the AZO nano-particles, had QE  $\sim 1.6$  times greater. This could be attributed to the plasmonic enhancement effect of the AZO nanoparticles on the local optical pump IR field. Since the upconversion emission is a two-photon process, QE could be increased proportional to approximately the square of the pump power. In this experiment the maximum pump power was limited to 150 mW, less than the damage threshold of the nano-composite film.

The reason for the nano-composite film having an order of magnitude weaker upconversion fluorescence than that of the bulk phosphor powder, besides a limited concentration of the phosphor

Table 1  
Quantum efficiency of different upconversion emitters (at 515 and 535 nm combined) used in the experiment.

No	Specimen	QE (%)
1	$\text{NaYF}_4: \text{Yb}^{3+}, \text{Er}^{3+}$ target	$0.56 \pm 0.12$
2	PMMA + $\text{NaYF}_4: \text{Yb}^{3+}, \text{Er}^{3+}$ nano-composite film	$0.045 \pm 0.013$
3	PMMA + $\text{NaYF}_4: \text{Yb}^{3+}, \text{Er}^{3+}$ + AZO nano-composite film	$0.072 \pm 0.022$

nano-particles in the polymer host, could be related to the size effect explained below. The molar mass of phosphor  $\text{NaYF}_4: \text{Yb}^{3+}, \text{Er}^{3+}$  was  $M = 187.9 \text{ g/Mole}$ . The mass density was  $\rho_m = 4.2 \text{ g/cm}^3$  [57]. The molar density  $\rho_M$  could be calculated as

$$\rho_M = \frac{\rho_m}{M} = 0.022 \frac{\text{Mole}}{\text{cm}^3} \quad (11)$$

Sodium concentration  $N_{\text{Na}}$  in the phosphor would be

$$N_{\text{Na}} = N_A \rho_M = 1.2 \times 10^{22} \frac{\text{ion}}{\text{cm}^3} \quad (12)$$

where  $N_A = 6.02 \times 10^{23} \text{ Mole}^{-1}$  is the Avogadro number. Since the doping rates of Ytterbium and Erbium were 10% and 2% respectively (see above), their concentrations in the phosphor would be  $N_{\text{Yb}} = 0.1 \rho_{\text{Na}} = 1.2 \times 10^{21} \text{ ion/cm}^3$  and  $N_{\text{Er}} = 0.02 \rho_{\text{Na}} = 2.4 \times 10^{20} \text{ ion/cm}^3$ . Assuming spherical shape of the nano-particles of the upconversion phosphor (with volume  $V = 1.33\pi(D/2)^3$ , where  $D$  is the diameter of the nano-particle), Table 2 presents the computed number of the RE ions in the nanoparticles of different sizes. One can see that the number of Ytterbium as well as Erbium ions in the nano-particles of 1-nm diameter is less than one in average and does not exceed several hundred in 10-nm nanoparticles. The upconversion emission involved two types of RE ions with the  $\text{Yb}^{3+}$  ion acting as a captor of the pump IR photons that later excited the  $\text{Er}^{3+}$  ion through the energy transfer process involving two IR photons, but not one. The upconversion emission thus relied on a significant number of the RE ions involved – no less than thousands. Accordingly, the nano-composite film including the nano-particles of the upconversion phosphor of the size not exceeding ~200 nm should expectedly have upconversion QE less than that of the bulk powder with significant presence of 1- $\mu\text{m}$  and greater particles. As Table 1 indicates, adding the nano-particles of AZO to the polymer nano-composite film helped to partially compensate the drop of upconversion QE due to the plasmon enhancement of the local pump IR optical field. As an illustration of possible applications for upconversion fiber illuminators, Fig. 13 presents the photograph of the tip of a single-mode fiber coated with the above-described MAPLE/PLD method with a nano-composite film of  $\text{PMMA} + \text{NaYF}_4: \text{Yb}^{3+}, \text{Er}^{3+} + \text{AZO}$  pumped with a 980-nm laser diode (125-mW power). The tip of the fiber illuminated the white back side of a business card with visible upconversion light. The picture was taken with an iPhone 6 digital camera at dimmed room light.

#### 4. Conclusions

It has been demonstrated for the first time that the proposed new triple-beam triple-target MAPLE/PLD deposition method made possible to transfer an efficient upconversion RE inorganic phosphor concurrently with AZO compound in nano-composite polymer films preserving crystalline structure of the additives and the upconversion emission properties. This is due to much

**Table 2**

Computed number of RE ions in the spherical nano-particles of the upconversion phosphor of different diameter.

No	Diameter of the spherical nano-particle of the upconversion phosphor in nm	Number of the rare earth ions in the nano-particle	
		$\text{Yb}^{3+}$	$\text{Er}^{3+}$
1	1	0.628	0.128
2	10	628	128
3	100	$6.28 \times 10^5$	$1.28 \times 10^5$
4	1000	$6.28 \times 10^8$	$1.28 \times 10^8$

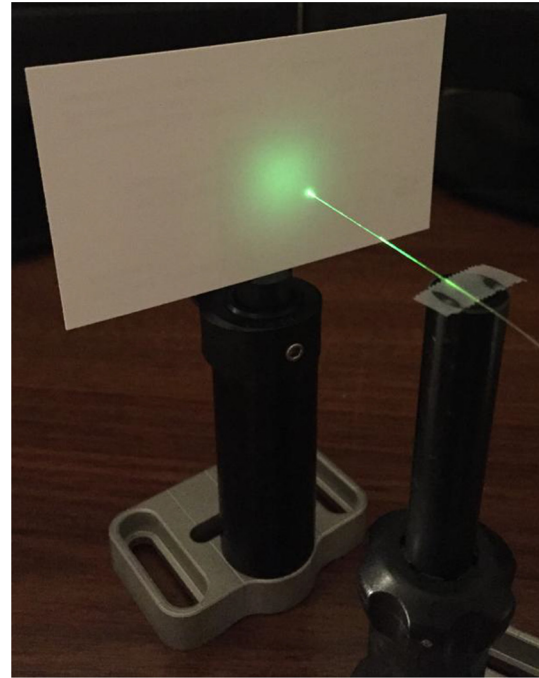


**Fig. 13.** Photograph of the tip of a single-mode fiber coated with a nano-composite film of  $\text{PMMA} + \text{NaYF}_4: \text{Yb}^{3+}, \text{Er}^{3+} + \text{AZO}$  pumped with a 980-nm laser diode (125-mW power) illuminating white back side of a business card.

better control of the deposition process of the materials of different nature of three separate targets with three different laser beams. The basic components of the new triple-beam triple-target MAPLE/PLD apparatus and the major process steps have been designed, built, and tested. The preliminary results indicated that adding AZO nano-particles improved by a factor of 1.6 the upconversion quantum efficiency of the upconversion emission from the films possibly due to the plasmon enhancement of the local optical pump IR field in the vicinity of the of AZO nano-particles. The proposed method can be potentially used for fabrication of a wide variety of nano-composite polymer-inorganic films for light emitters, chemical sensors, and other applications.

#### Acknowledgements

The authors would like to acknowledge the support from DOD, United States grants FA 9550-12-1-0068, W911NF-11-1-0192, W911-15-1-0446, W911-16-1-0502, United States NSF HRD# 1002541 and Paolo Mele acknowledges partial financial support from Japan of Kakenhi (C) grant No. 26390103.

#### References

- [1] Mihaiescu DE, Cristescu R, Dorcioman G, Popescu CE, Nita C, Socol G, et al. Functionalized magnetite silica thin films fabricated by MAPLE with antibiofilm properties. *Biofabrication* 2013;5(1):015007.
- [2] Paun IA, Moldovan AM, Luculescu C, Dinescu M. Antibacterial polymeric coatings grown by matrix assisted pulsed laser evaporation. *Appl Phys A Mater Sci Process* 2013;110(4):895–902.
- [3] Shepard KB, Guo Yunlong, Arnold CB, Priestley RD. Nanostructured morphology of polymer films prepared by matrix assisted pulsed laser evaporation. *Appl Phys A Mater Sci Process* 2013;110(4):771–7.
- [4] Shepard KB, Priestley RD. MAPLE Deposition of macromolecules. *Macromol Chem Phys* 2013;214(8):862–72.
- [5] Iordache S, Cristescu R, Popescu AC, Popescu CE, Dorcioman G, Mihaiescu IN, et al. Functionalized porphyrin conjugate thin films deposited by matrix assisted pulsed laser evaporation. *Appl Surf Sci* 8:207–210.
- [6] Singaravelu S, Mayo DC, Park HK, Schriver KE, Haglund Jr RF. Anti-reflective polymer-nanocomposite coatings fabricated by RIR-MAPLE. *Proc SPIE*

- 2013;8607:860718.
- [7] Shepard KB, Arnold CB, Priestley RD. Origins of nanostructure in amorphous polymer coatings via matrix assisted pulsed laser evaporation. *Appl Phys Lett* 2013;103(12):123105.
  - [8] Caricato AP, Arima V, Cesaria M, Martino M, Tunno T, Rinaldi R, et al. Solvent-related effects in MAPLE mechanism. *Appl Phys B Lasers Opt* 2013;113(3):463–71.
  - [9] Birjega R, Matei A, Mitu B, Ionita MD, Filipescu M, Stokker-Cheregi F, et al. Layered double hydroxides/polymer thin films grown by matrix assisted pulsed laser evaporation. *Thin Solid Films* 2013;543:63–8.
  - [10] McCormick RD, Cline ED, Chadha AS, Zhou W, Stiff-Roberts AD. Tuning the refractive index of homopolymer blends by controlling nanoscale domain size via RIR-MAPLE deposition. *Macromol Chem Phys* 2013;214(23):2643–50.
  - [11] Canulescu S, Schou J, Fester S, Hansen KV, Conseil H. Deposition of matrix-free fullerene films with improved morphology by matrix-assisted pulsed laser evaporation (MAPLE). *Chem Phys Lett* 2013;588:119–23.
  - [12] Visan A, Grossin D, Stefan N, Duta L, Miroiu FM, Stan GE, et al. Biomimetic nanocrystalline apatite coatings synthesized by Matrix Assisted Pulsed Laser Evaporation for medical applications. *Mat Sci Eng B Adv Funct Solid-State Mater* 2014;181:56–63.
  - [13] Stokker-Cheregi F, Matei A, Dinescu M, Secu CE, Secu M. Photoluminescence of Eu-doped LiYF<sub>4</sub> thin films grown by pulsed laser deposition and matrix-assisted pulsed laser evaporation. *J Phys D Appl Phys* 2014;47(4):045304.
  - [14] Constantinescu C, Matei A, Ion V, Mitu B, Ionita I, Dinescu M, et al. Ferrocene carboxaldehyde thin films grown by matrix-assisted pulsed laser evaporation for nonlinear optical applications. *Appl Surf Sci* 2014;302:83–6.
  - [15] Palla-Papavlu A, Rusen L, Dinca V, Filipescu M, Lippert T, Dinescu M. Characterization of ethylcellulose and hydroxypropyl methylcellulose thin films deposited by matrix-assisted pulsed laser evaporation. *Appl Surf Sci* 2014;302:87–91.
  - [16] Grumezescu V, Socol G, Grumezescu AM, Holban AM, Ficai A, Bleotu C, et al. Functionalized antibiofilm thin coatings based on PLA-PVA microspheres loaded with usnic acid natural compounds fabricated by MAPLE. *Appl Surf Sci* 2014;302:262–7.
  - [17] Rusen L, Dinca V, Mitu B, Mustaciosu C, Dinescu M. Temperature responsive functional polymeric thin films obtained by matrix assisted pulsed laser evaporation for cells attachment-detachment study. *Appl Surf Sci* 2014;302:134–40.
  - [18] Caricato AP, Arima V, Catalano M, Cesaria M, Cozzoli PD, Martino M, et al. MAPLE deposition of nanomaterials. *Appl Surf Sci* 2014;302:92–8.
  - [19] Socol M, Preda N, Vacareanu L, Grigoras M, Socol G, Mihailescu IN, et al. Organic heterostructures based on arylenevinylene oligomers deposited by MAPLE. *Appl Surf Sci* 2014;302:216–22.
  - [20] Constantinescu C, Matei A, Ionita I, Ion V, Marascu V, Dinescu M, et al. Azoderivatives thin films grown by matrix-assisted pulsed laser evaporation for non-linear optical applications. *Appl Surf Sci* 2014;302:69–73.
  - [21] Grumezescu V, Holban AM, Grumezescu AM, Socol G, Ficai A, Vasile BS, et al. Usnic acid-loaded biocompatible magnetic PLGA-PVA microsphere thin films fabricated by MAPLE with increased resistance to staphylococcal colonization. *Biofabrication* 2014;6(3):035002.
  - [22] Sima F, Axente E, Iordache I, Luculescu C, Gallet O, Anselme K, et al. Combinatorial Matrix Assisted Pulsed Laser Evaporation of a biodegradable polymer and fibronectin for protein immobilization and controlled release. *Appl Surf Sci* 2014;306:75–9.
  - [23] Grumezescu V, Holban AM, Iordache F, Socol G, Mogosanu GD, Grumezescu V, et al. MAPLE fabricated magnetite-eugenol and (3-hydroxybutyric acid-co-3-hydroxyvaleric acid)-polyvinyl alcohol microspheres coated surfaces with anti-microbial properties. *Appl Surf Sci* 2014;306:16–22.
  - [24] Axente E, Sima F, Sima LE, Erginer M, Eroglu MS, Serban N, et al. Combinatorial MAPLE gradient thin film assemblies signaling to human osteoblasts. *Biofabrication* 2014;6(3):035010.
  - [25] Dinca V, Florian PE, Sima LE, Rusen L, Constantinescu C, Evans RW, et al. MAPLE-based method to obtain biodegradable hybrid polymeric thin films with embedded antitumoral agents. *Biomed Microdevices* 2014;16(1):11–21.
  - [26] Ge Wangyao, Yu Qian, Lopez GP, Stiff-Roberts AD. Antimicrobial oligo(p-phenylene-ethynylene) film deposited by resonant infrared matrix-assisted pulsed laser evaporation. *Colloids Surfaces B Biointerfaces* 2014;116:786–92.
  - [27] Aronne A, Ausanio G, Bloisi F, Calabria R, Califano V, Fanelli E, et al. Structural characterization of MAPLE deposited lipase biofilm. *Appl Surf Sci* 2014;320:524–30.
  - [28] Califano V, Bloisi F, Aronne A, Federici S, Nasti L, Depero LE, et al. Biosensor applications of MAPLE deposited lipase. *Biosensors* 2014;4(4):329–39.
  - [29] Yu Qian, Ge Wangyao, Atewologun A, Lopez GP, Stiff-Roberts AD. RIR-MAPLE deposition of multifunctional films combining biocidal and fouling release properties. *J Mat Chem B* 2014;2(27):4371–8.
  - [30] Constantinescu C, Rotaru A, Nedelcea A, Dinescu M. Thermal behavior and matrix-assisted pulsed laser evaporation deposition of functional polymeric materials thin films with potential use in optoelectronics. *Mat Sci Semicond Process* 2015;30:242–9.
  - [31] Caricato AP, Cesaria M, Leo C, Mazzeo M, Genco A, Carallo S, et al. Very low roughness MAPLE-deposited films of a light emitting polymer: an alternative to spin coating. *J Phys D Appl Phys* 2015;48(13):135501.
  - [32] Aronne A, Bloisi F, Calabria R, Califano V, Depero LE, Fanelli E, et al. Lipase biofilm deposited by matrix assisted pulsed laser evaporation technique. *Appl Surf Sci* 2015;336:196–9.
  - [33] Iordache F, Grumezescu V, Grumezescu AM, Curtiu C, Ditu LM, Socol M, et al. Gamma-cyclodextrin/usnic acid thin film fabricated by MAPLE for improving the resistance of medical surfaces to *Staphylococcus aureus* colonization. *Appl Surf Sci* 2015;336:407–12.
  - [34] Matei A, Constantinescu C, Mitu B, Filipescu M, Ion V, Ionita I, et al. Laser printing of azo-derivative thin films for non-linear optical applications. *Appl Surf Sci* 2015;336:200–5.
  - [35] Stiff-Roberts AD, McCormick RD, Ge Wangyao. Material properties and applications of blended organic thin films with nanoscale domains deposited by RIR-MAPLE. *Proc SPIE* 2015;9350:935007.
  - [36] Grumezescu V, Andronescu E, Holban AM, Grumezescu AM, Socol G, Iordache F, et al. MAPLE fabrication of thin films based on kanamycin functionalized magnetite nanoparticles with anti-pathogenic properties. *Appl Surf Sci* 2015;336:188–95.
  - [37] Caricato AP, Anni M, Cesaria M, Lattante S, Leggieri G, Leo C, et al. MAPLE-deposited PFO films: influence of the laser fluence and repetition rate on the film emission and morphology. *Appl Phys B Lasers Opt* 2015;19(3):453–61.
  - [38] Ge Wangyao, Atewologun A, Stiff-Roberts AD. Hybrid nanocomposite thin films deposited by emulsion-based resonant infrared matrix-assisted pulsed laser evaporation for photovoltaic applications. *Org Electron Mater Phys Chem Appl* 2015;22:98–107.
  - [39] Janković A, Eraković S, Ristoscu C, Mihailescu N, Duta L, Visan A, et al. Structural and biological evaluation of lignin addition to simple and silver-doped hydroxyapatite thin films synthesized by matrix-assisted pulsed laser evaporation. *J Mater Sci Mater Med* 2015;26(1):17.
  - [40] Paun IA, Acasandrei AM, Luculescu CR, Mustaciosu CC, Ion V, Mihailescu M, et al. MAPLE deposition of polypyrrole-based composite layers for bone regeneration. *Appl Surf Sci* 2015;357:975–84.
  - [41] Darwish AM, Sagapolutele MT, Sarkisov S, Patel D, Hui D, Koplitz B. Double beam pulsed laser deposition of composite films of poly(methyl methacrylate) and rare earth fluoride upconversion phosphors. *Compos Part B Eng* 2013;55:139–46.
  - [42] Darwish AM, Wilson S, Sarkisov S, Patel D. Double pulse laser deposition of polymer nanocomposite NaYF<sub>4</sub>:Tm<sup>3+</sup>, Yb<sup>3+</sup> films for optical sensors and light emitting applications. *Proc SPIE* 2014;8847:884702.
  - [43] Darwish AM, Burkett A, Blackwell A, Taylor K, Sarkisov S, Patel D, et al. Polymer-inorganic nano-composite thin film upconversion light emitters prepared by double-beam matrix assisted pulsed laser evaporation (DB-MAPLE) method. *Compos Part B* 2015;68:355–64.
  - [44] Darwish AM, Burkett A, Blackwell A, Taylor K, Walker V, Sarkisov S, et al. Efficient upconversion polymer-inorganic nanocomposite emitters prepared by the double beam matrix assisted pulsed laser evaporation (DB-MAPLE). *Proc SPIE* 2014;9200:92000C.
  - [45] Darwish AM, Wilson S, Blackwell A, Taylor K, Sarkisov SS, Patel DN, et al. Ammonia Sensor based on polymer-inorganic nano-composite thin film upconversion light emitter prepared by double-beam pulsed laser deposition. *Am J Mater Sci* 2015;5(3A):8–15.
  - [46] Darwish AM, Wilson S, Blackwell A, Taylor K, Sarkisov S, Patel D, et al. Polymer-inorganic nanocomposite thin film emitters, optoelectronic chemical sensors, and energy harvesters produced by multiple-beam pulsed laser deposition. *Proc SPIE* 2015;9586:958602.
  - [47] Darwish AM, Wilson S, Blackwell A, Taylor K, Sarkisov S, Patel D, et al. Multi-beam pulsed laser deposition: new method of making nanocomposite coatings. *Proc SPIE* 2015;9586:958605.
  - [48] Darwish A, Sarkisov S. Multiple beam pulsed laser deposition of composite films, US Patent Application No. 14/158,567, Filed 1/17/2014, Publication No. US 2014/0227461 A1.
  - [49] Darwish A, Sarkisov S. Multiple beam pulsed laser deposition of composite films, US Patent Application No. 14/506,685, Filed 10/15/2014.
  - [50] Darwish A, Mele P, Sarkisov S. Nano-composite thermo-electric energy converter and fabrication method thereof. US Patent Application No. 14/853,674, Filed 9/14/2015.
  - [51] West PR, Ishii S, Naik GV, Emani NK, Shalaeva VM, Boltasseva A. Searching for better plasmonic materials. *Laser Photonics Rev* 2010;4(6):795–808.
  - [52] Kim Y, Lee W, Jung D-R, Kim J, Nam S, Kim H, et al. Optical and electronic properties of post-annealed ZnO: Al thin films. *Appl Phys Lett* 2010;96(17):171902.
  - [53] Tong H, Deng Z, Liu Z, Huang C, Huang J, Lan H, et al. Effects of post-annealing on structural, optical and electrical properties of Al-doped ZnO thin films. *Appl Surf Sci* 2011;257(11):4906–11.
  - [54] Lin J-Y, Zhong K-D, Lee P-T. Plasmonic behaviors of metallic AZO thin films and AZO nanodisk arrays. *Opt Express* 2016;24(5):5125.
  - [55] Cullity BD, Stock SR. Elements of X-ray diffraction. 3rd ed. Prentice Hall; 2001.
  - [56] Boyer JCh, van Veggel FCJM. Absolute quantum yield measurements of colloidal NaYF<sub>4</sub>: Er<sup>3+</sup>, Yb<sup>3+</sup> upconverting nanoparticles. *Nanoscale* 2010;2:1417–9.
  - [57] Liu H, Xu CT, Dumlupinar G, Jensen OB, Andersen PE, Andersson-Engels S. Deep tissue optical imaging of upconverting nanoparticles enabled by exploiting higher intrinsic quantum yield through use of millisecond single pulse excitation with high peak power. *Nanoscale* 2013;20(5):10034–40.